frontiers | Frontiers in Marine Science

TYPE Original Research
PUBLISHED 17 August 2022
DOI 10.3389/fmars.2022.902815

OPEN ACCESS

EDITED BY
Hermann Ehrlich,
Freiberg University of Mining and Technology, Germany

REVIEWED BY
Jose Luis Arias,
University of Chile, Chile
Marcin Wysokowski,
Poznań University of Technology, Poland

*CORRESPONDENCE
Pei-Yuan Qian
boqianpy@ust.hk
Ning Wang
phwang@ust.hk

SPECIALTY SECTION
This article was submitted to Marine Molecular Biology and Ecology, a section of the journal Frontiers in Marine Science

RECEIVED 23 March 2022
ACCEPTED 25 July 2022
PUBLISHED 17 August 2022

CITATION
Ying Z, Wang S, Wong WC, Cai X, Feng X, Xiang S, Cai Y, Qian P-Y and Wang N (2022) An insight into the microstructures and composition of 2,700-m-depth deep-sea limpet shells. *Front. Mar. Sci.* 9:902815. doi: 10.3389/fmars.2022.902815

An insight into the microstructures and composition of 2,700 m-depth deep-sea limpet shells

Zhehan Ying[1,2,3], Shi Wang[1,2], Wai Chuen Wong[2,4], Xiangbin Cai[1,2], Xuemeng Feng[1], Shengling Xiang[1,2], Yuan Cai[1], Pei-Yuan Qian[2,4]* and Ning Wang[1,2]*

[1]Department of Physics and William Mong Institute of Nano Science and Technology, The Hong Kong University of Science and Technology, Hong Kong, Hong Kong SAR, China, [2]Southern Marine Science and Engineering Guangdong Laboratory (Guangzhou), Guangzhou, China, [3]Materials Characterization and Preparation Facility (Guangzhou), The Hong Kong University of Science and Technology (Guangzhou), Guangzhou, China, [4]Department of Ocean Science, The Hong Kong University of Science and Technology, Hong Kong, Hong Kong SAR, China

Structural and physiochemical properties contribute to the biological adaptation of deep-sea animals to their harsh living environment but have hardly been investigated systematically. In the present study, we for the first time applied various material characterization techniques including transmission electron microscopy (TEM), scanning electron microscopy (SEM), energy-dispersive X-ray spectroscopy (EDS), X-ray diffraction (XRD), and Fourier-transform infrared (FT-IR) spectroscopy to investigate the shell microstructures and chemical composition of a deep-sea limpet *Eulepetopsis crystallina* collected from the Tiancheng hydrothermal vent field at a depth of around 2,700 m in the Southwest Indian Ocean. Analyses of shell microstructural morphology and diffraction patterns of *E. crystallina* explicitly revealed the layered structures, exfoliation characteristics, and crystallographic orientation of each layer's unit cell which was tilted at a small angle sequentially. In comparison with ordinary shallow-water limpet *Cellana toreuma* shells, *E. crystallina* shells showed a unique chemical composition and contained pure calcite of calcium carbonate polymorph and the trace of phosphate originated from regional phosphatic sediments of the Southwest Indian Ocean. The further microscopic analyses indicated that the shell of the deep-sea limpet *E. crystallina* features integrated and untruncated layer structures with a compressed width, possibly owning to the ultra-high hydrostatic pressure, which confirmed the effects of the living environment on the shell microstructure of deep-sea animals.

KEYWORDS

Deep-sea, limpet, microstructure, composition, crystallography

Introduction

The microstructure and chemical composition of the deep-sea limpet shells have been investigated, which serves as the first step to investigate their formation mechanism and adaptation to the deep-sea environment (Nakai et al., 2006; Suzuki et al., 2010; Rodolfo-Metalpa et al., 2011; Li et al., 2015). The shell of limpet (Gastropoda class: aquatic snails) features as a composite biomaterial with multifunctional roles in providing mechanical strength and protective support to sustain the life activities of limpet (Denny, 2000; Harley et al., 2009; Johnson et al., 2019). Shallow-water limpets normally gather on the rocky shores where sea waves sweep over them. The flows exert a strong lift or drag force on the shell structures, and thus, shell microstructures need to withstand and adapt to the effects of water velocity in excess of 20 m/s (Denny, 2000). The main chemical composition of limpet shells is composed of calcium carbonate polymorphs and potential inorganic trace elements (Carroll and Romanek, 2008; Agbaje et al., 2018). The morphology, size, color, transparency, and even microstructures of the calcareous shells show remarkable distinction at different depths of the sea (Checa et al., 2006). Accordingly, compared with the common shallow-water limpet shells, the deep-sea limpet shells are expected to be distinctive in their microstructures and physicochemical characteristics because the animals usually live in an environment with relatively slow water velocity—but totally dark—and high hydrostatic pressure. Information on the shell microstructure and physiochemistry will provide insights into their functional properties and biomimetic applications that allow selection as prospective biomaterials.

The formation of limpet shell has been determined as a typical process of biomineralization (Weiner and Addadi, 2011; Oliveira et al., 2020), in which calcium carbonate evolves in different crystalline polycrystalline forms, such as calcite, aragonite, and spheraragonite, under natural conditions (Song et al., 2019). The various crystalline polycrystals of calcium carbonate are arranged in layers with unique patterns to form complex biomineral microstructures in limpet shells. In previous studies, the shallow-water limpet *Patella pellucida* (depth<27 m) featuring the blue-rayed translucent shell was proven to be an embedded hierarchical photonic architecture which displayed the light reflection from the exterior shell (Li et al., 2015). Besides, the shallow-water limpet *Patella vulgate* shell showed strong impact resistance, which depends on the two geometric parameters: apex thickness and the ratio of apex height to rim diameter (Harford et al., 2020). Up to now, the relevant research on limpet shells has mainly focused on the shallow-water species, and thus, there has been limited information on shell microstructures and chemical composition of highly structured biomineralized deep-sea animal shells.

In this study, we aimed to reveal the shell microstructures and chemical composition of the deep-sea limpet *E. crystallina* living at a depth of about 2,700 m of the Southwest Indian Ocean Ridge using various material characterization techniques including transmission electron microscopy (TEM), scanning electron microscopy (SEM), energy-dispersive X-ray spectroscopy (EDS), X-ray diffraction (XRD), and Fourier-transform infrared (FT-IR) spectroscopy. The TEM characterization is a proficient tool that allows scientists to investigate microstructural images and crystallographic details of nanomaterials (Suzuki et al., 2011; Suzuki et al., 2017; Wang et al., 2018; Ying et al., 2020). The width difference in layered structure between *E. crystallina* and *C. toreuma* shells due to their living environment was determined by TEM images. The SEM which scans a focused electron beam on the material surface can provide information about the surface morphology and layered microstructures of shells. Besides, the chemical composition of deep-sea and shallow-water limpet shells was explicitly determined. EDS is feasible for elemental analysis which analyzes the characteristic X-ray emission spectra from the individual element (Ying et al., 2021b). FT-IR detects the infrared spectrum of absorption or emission of samples and determines the bonding characteristics of inorganic materials. Non-destructive XRD offers detailed information of crystallographic structures, lattice parameters, and chemical composition. By EDS and FT-IR, the trace of phosphate was detected in shells of deep-sea limpet *E. crystallina*, but not in shallow-water limpet *C. toreuma*. Therefore, these exhaustive investigations on *E. crystallina* shells will give insight into shell microstructures and chemical compositions of deep-sea limpets, providing a wide range of possibilities for limpet living environments, shell formation mechanism, origin of invertebrate marine biomaterials, forced biomineralization, and extreme biomimetics (Li et al., 2015; Ehrlich and Nikolaev, 2017; Ehrlich, 2019; Lomovasky et al., 2020; Ehrlich et al., 2021).

Materials and methods

Collection of deep-sea limpets from the Southwest Indian Ocean and shallow-water limpets from Hong Kong

Deep-sea limpets *Eulepetopsis crystallina* were collected using the ROV *Sea Dragon III* onboard the R/V *Dayangyihao* from the Tiancheng hydrothermal vent field in the Southwest Indian Ocean during the COMRA DY52nd cruise in April 2019 (see details in Sun et al., 2020) (Sun et al., 2020). The deep-sea limpet *E. crystallina* samples were stored at −80°C after collections. Samples were directly fixed in pure ethanol immediately after arrival onboard. Soft tissues were removed from the shells with tweezers in the laboratory; the remaining shells were immersed in 0.2% of bleach and gently shaken at a rotation speed of 250 rpm at room temperature for 2 h to further

remove the residual of soft tissues, and the shaking process was repeated with 0.1% of bleach and rinsed with Milli-Q waters.

Shallow-water limpets *Cellana toreuma* were manually collected from the shore of Clear Water Bay in The Hong Kong University of Science and Technology, Hong Kong, in October 2019. The shallow-water limpet *C. toreuma* samples were stored at -80°C after collections. After arrival onboard, samples were rinsed with water and fixed in pure ethanol immediately on the collection site. Soft tissues were removed from the shells with tweezers in the laboratory, the remaining shells were immersed in 0.2% of bleach and gently shaken at a rotation speed of 250 rpm at room temperature for 2 h to further remove the residual of soft tissues, and the shaking process was repeated with 0.1% of bleach and rinsed with Milli-Q water.

Besides, the limpet *E. crystallina* and *C. toreuma* samples were stored at -80°C and then conducted for microstructure characterization and chemical composition analysis after the ROV *Sea Dragon III* arrived at the home port and treatments in the laboratory (approximately 2 months later).

The microstructure characterization

For the samples characterized by TEM and SEM, the ultra-thin lamella samples of shells of both the deep-sea limpet *E. crystallina* and shallow-water limpet *C. toreuma* were prepared through the milling and fabrication processes using the FEI dual-beam FIB/FESEM system (Helios G4 UX, Waltham, United States), which enabled cross-sectional milling and imaging to reveal microstructures below the surfaces. The equipped drift compensated frame integration (DCFI) and Thermo Scientific SmartScan^{TM} modes can realize integrated sample cleanliness management and dedicated imaging modes, which offered artifact-free imaging. The low-dose condition was applied in the FIB process to eliminate the potential Ga^+ beam-induced damage. The selected area electron diffraction (SAED) and high-resolution TEM (HRTEM) images that disclosed the crystallographic information and layered microstructures of the deep-sea and shallow-water limpet shells were captured by a JEOL 2010F field emission gun transmission electron microscope working at 200 kV with the point-to-point resolution of 1.2 Å. All TEM images were captured under electron beam fux with a current density of less than 20 pA/cm^2, in order to protect the sample from electron irradiation damage such as knock-on damage and thermal effect (Ying et al., 2021c). The morphology images were provided by the JEOL-6390 SEM and FEI dual-beam FIB/FESEM system (Helios G4 UX, Waltham, United States) working at 20 kV.

The chemical composition analysis

The EDS spectra of the chemical compositions of deep-sea and shallow-water limpet shells were characterized using the EDS system and using a 65-mm^2 Oxford Silicon Drift Detector (SDD, Abingdon, UK) – X-Max with the resolution of 133 eV which was directly connected with HRTEM. The XRD spectra of deep-sea and shallow-water shells were characterized using a Powder X-ray PANalytical diffractometer (X'Pert Pro, Malvern, UK) equipped with a Cu Kα1 X-ray emitting source, λ = 1.5406 Å. The infrared spectra of deep-sea and shallow-water shells were characterized using the Bruker Vertex 70 Hyperion 1000 FT-IR spectrometer over a range of 4000 cm^{-1} to 400 cm^{-1} at a 2-cm^{-1} resolution and averaging 64 scans.

Results

Optical microscope

The appearance, morphology, and exfoliation properties of *E. crystallina* and *C. toreuma* shells were first investigated under the optical microscope (Figure 1). The appearances of the *E. crystallina* shell and the *C. toreuma* shell are shown in Figures 1A, B where the *E. crystallina* shell exhibited a semitransparent shell structure while the *C. toreuma* shell featured a brown and opaque structure. Under the optical microscope, the *E. crystallina* shell exhibited an uneven and semitransparent lamellar structure (Figure 1C) while the *C. toreuma* shell showed a smooth and dense surface (Figure 1D). The interference in Figure 1C results from the overlapped and uneven layer structures of *E. crystallina* shells. The interference fringes shown in the optical image of *E. crystallina* shell surface (Figure 1C) indicated that its distinct layered microstructure has endowed it with this light reflection property. In Figure 1D, the complete triangular shape is attributed to cleavage which is the tendency preference of crystalline materials to split along defined crystallographic structural planes. The observed smooth repeating surfaces under the optical microscope resulted from the regular locations of atoms and ions in crystalline materials. When the bonds in certain directions are weaker than those in others, the crystal will tend to split along these weakly bonded planes, which leads to the complete and smooth triangular shape of shallow-water limpet *C. toreuma* shell. These flat breakages are termed "cleavage." Due to the resolution limit, the more detailed microscopic structure cannot be observed by optical microscopy; thus, further observation will be required with electron microscopy. Besides, several-layer or even single-layer lamella of the *E. crystallina* shell can be readily prepared by mechanical exfoliation (pointed out by arrows in Figure 1E) in which the fresh surface of layered shells was torn off using an adhesive tape. This exfoliation phenomenon was attributed to the very weak van der Waals interaction between the layers of the deep-sea limpet *E. crystallina* shell. However, this unique exfoliation availability was not achieved in *C. toreuma* shells (pointed out by arrows in Figure 1F).

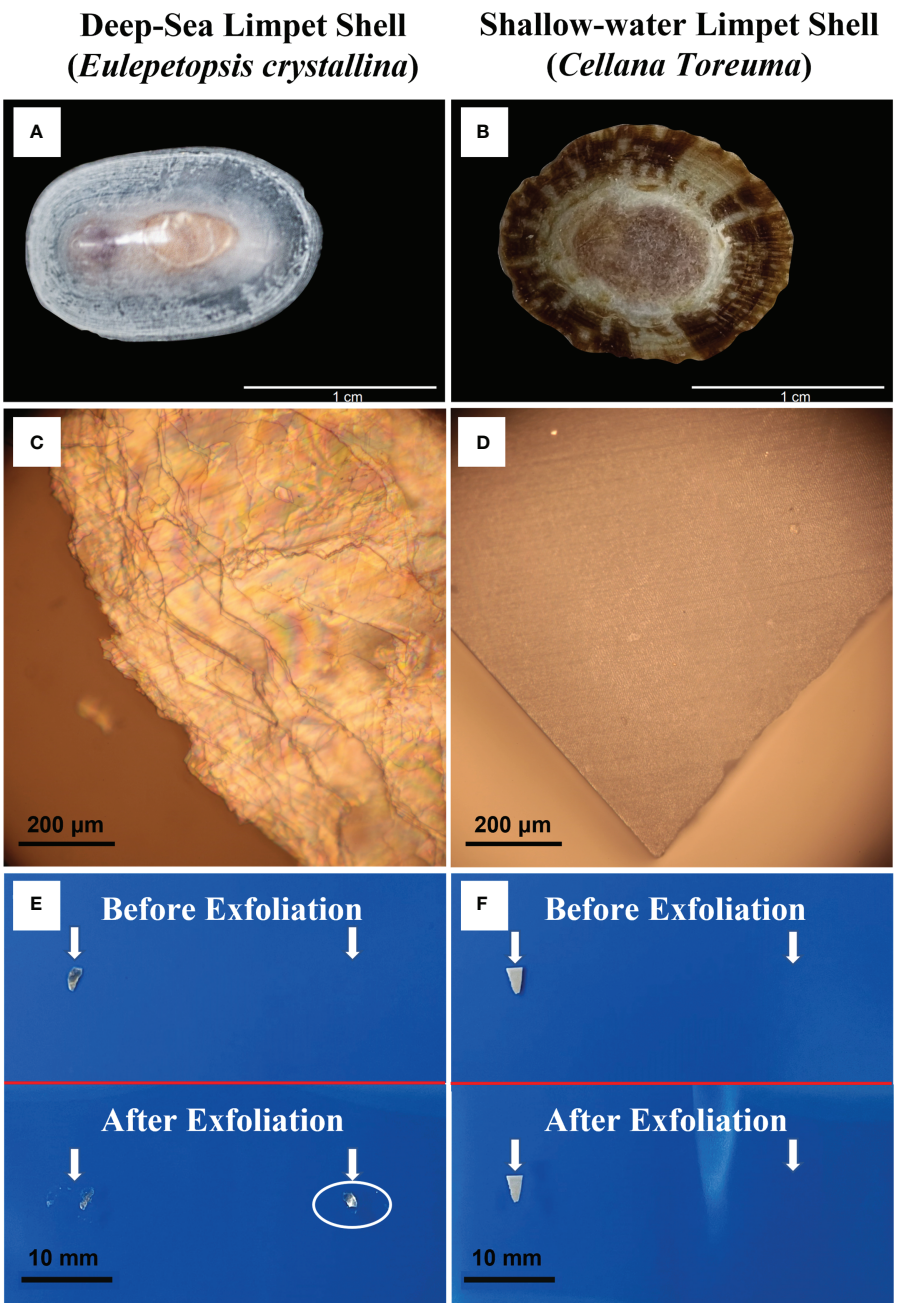

FIGURE 1
Optical images of **(A)** deep-sea limpet *E. crystallina* shell; **(B)** shallow-water limpet *C. toreuma* shell; **(C)** *E. crystallina* shell surface showing evident interference fringes; **(D)** *C. toreuma* shell dense and smooth surface; **(E)** visible exfoliation property of deep-sea limpet *E. crystallina* shell structure before and after exfoliation, and **(F)** shallow-water limpet *C. toreuma* shell structure before and after exfoliation. [Photos Figure 1A courtesy of Dr. Chenggang Liu].

TEM

The high-magnification morphology and microstructures of *E. crystallina* shells shown in the TEM images at different magnifications (Figure 2) explicitly revealed the microstructural details and exfoliation availability of layered structures. In the plane-view TEM image (Figure 2A), a thin layer can be exfoliated from the base and subsequently folded on the top layer (outlined by yellow dot line), which can be confirmed by the Moiré patterns at the overlaying area. The Moiré patterns are the interference patterns that are produced when the crystalline nanosheet pattern is overlaid on the adjacent similar pattern, and thus they are the most direct

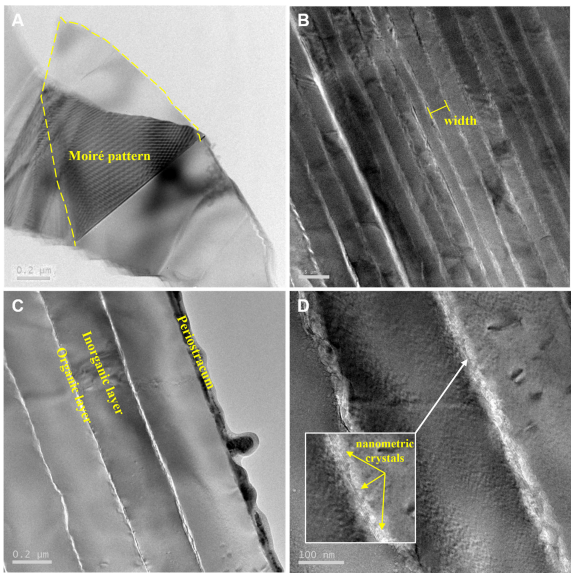

FIGURE 2
TEM images of deep-sea limpet *E. crystallina* shells at a depth of 2,700 m in the Southwest Indian Ocean. **(A)** Plane-view image showing the exfoliation property of the *E. crystallina* shell; **(B–D)** cross-sectional images showing multilayered microstructures of *E. crystallina* shells at different magnifications.

features for exfoliation properties under microscopic imaging (Jiang et al., 2014). In the cross-sectional TEM images (Figures 2B, C), alternate inorganic–organic layers protected by the outermost organic periostracum were clearly observed in the *E. crystallina* shell. Due to mass-thickness contrast, the inorganic crystal parts were observed as thicker and darker layers and separated by the organic parts as thinner and brighter layers. In the TEM image of the cross-sectional areas of the *C. toreuma* limpet shell (Figure S1), the multilayered microstructure was clearly revealed, and the average thickness ($\bar{T}$) of organic matrices of the *C. toreuma* limpet shell was more inconspicuous and much thinner than those of deep-sea limpet *E. crystallina* shells ($\bar{T}_{C.\,toreuma}$ = 9nm < $\bar{T}_{E.\,crystallina}$ = 41nm) shown in Figure 2C, Figure S1. In the high-resolution TEM inset image (Figure 2D), some lattice fringes were found in interfacial organic layers, indicating the presence of some inorganic nanometric crystals in the organic layer of *E. crystallina* shells. However, the lattice fringes of nanometric crystals were not found in the thin organic matrices of shallow-sea limpet *C. toreuma* shells.

SEM

The cross-sectional view of the *C. toreuma* shell (Figures 3A, B) exhibits a trilayered structure: the outermost thin organic matrix (periostracum) and two calcified layers (the outer prismatic layer and the inner nacreous layer). Compared with the *E. crystallina* shell, the *C. toreuma* shell features the different microstructures of prismatic layers. The crystal structures of the prismatic layers in the *E. crystallina* shell (Figure 3E) exhibit the integrated and untruncated layer structures without any cracks. In comparison, the prismatic layers of *C. toreuma* shells are made up of elongated calcified crystals, organized in the brick wall-like structures which feature interstitial cracks between adjacent crystal blocks (Figure 3D) (Marie et al., 2012). In Figures 3C, G, it is evident that the average width of inorganic crystal structures in the prismatic layer of *E. crystallina* shells ($\bar{w}_{E.\,crystallina}$ = 0.23μm) is far smaller than those of the *C. toreuma* shell ($\bar{w}_{C.\,toreuma}$ = 1.60μm), which is attributed to the ultra-high compressive force exerted by the hydrostatic pressure in the deep-sea environment at a depth of 2,700 m.

SAED

The selected-area electron diffraction (SAED) pattern was performed by TEM to determine the crystal structure and

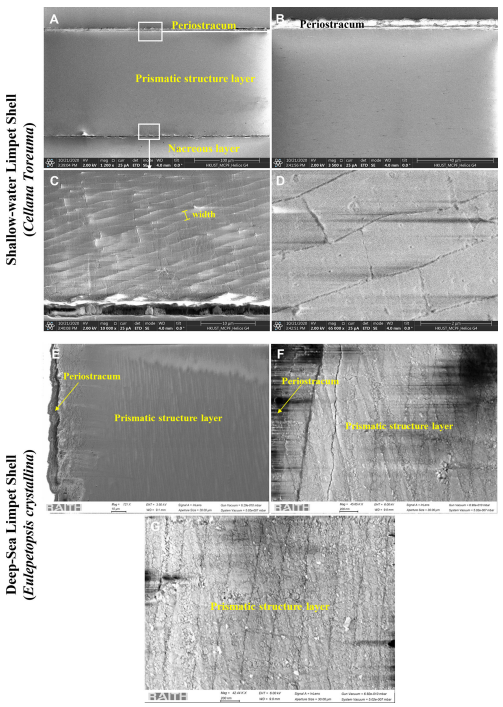

FIGURE 3
SEM images of the cross-sectional areas of shallow-water limpet *C. toreuma* shells prepared by FIB: **(A)** morphology of the cross-sectional layered structures. **(B)** The enlarged details of the relative area pointed by white rectangular frame (upper) in panel **(A)**. **(C)** The enlarged details of the relative area pointed by white rectangular frame (bottom) in panel **(A)**. **(D)** The high-magnification details of the prismatic structure layer in panel **(C)**; SEM images of cross-sectional areas of deep-sea limpet *E. crystallina* shells prepared by FIB: **(E)** morphology of the cross-sectional layered structures. **(F)** The enlarged details of the interface between the periostracum and prismatic structure layer. **(G)** The enlarged details of the prismatic structure layer.

crystallographic orientation of the layered structure of *E. crystallina* shells. Figure 4A exhibits a typical cross-sectional TEM image of the inorganic phase of *E. crystallina* shell, and the outermost inorganic structure of the prismatic layer outlined by yellow lines is selected for SAED characterization. Figure 4B shows the corresponding SAED pattern, where the diffraction spots confirm that the prismatic layer of *E. crystallina* shell is crystalline. The indexed SAED pattern verifies that the outermost inorganic layer has a trigonal calcite-$CaCO_3$ structure where the spacing of reciprocal lattice in Figure 4B matches with the calcite-$CaCO_3$ structure and the longitudinal orientation of the elongated outermost layer labeled by the white arrow is along the [0 0 0 6] direction. The unit cells of calcite are aligned in a texturized arrangement in the way that the c-axes are perpendicular to the lamella surface and others are horizontal to the lamella surface. Besides, the resulted lattice parameters are $a = 4.98$ Å, $c = 17.07$ Å, which are consistent with literature values, and the calcite crystals orient along the [$\bar{1}$ 0 1 0] zone axis (shown by the schematic model in the inset of Figure 4A) (Aizenberg et al., 1997). In Figure 5, in addition to the outermost calcite layer (labeled 1), four more SAED patterns of the inner layers (labeled 2–5) are recorded as shown in Figures 5C–F to investigate crystal orientation in these layers. Each diffraction spot in TEM images corresponded to a specifically satisfied diffraction condition of the sample's crystal structure. If the crystal is tilted, different diffraction conditions will be satisfied and diffraction spots will change. Here, for the layered structures 1–5, they exhibit different SAED patterns, which indicated that the crystal orientations of adjacent layered structures 1–5 are not aligned and tilted at a small angle sequentially. In addition, the information of SAED patterns of the shallow-water limpet *C. toreuma* shell (Figures 5G–J) was added and further compared with deep-sea limpet *E. crystallina*

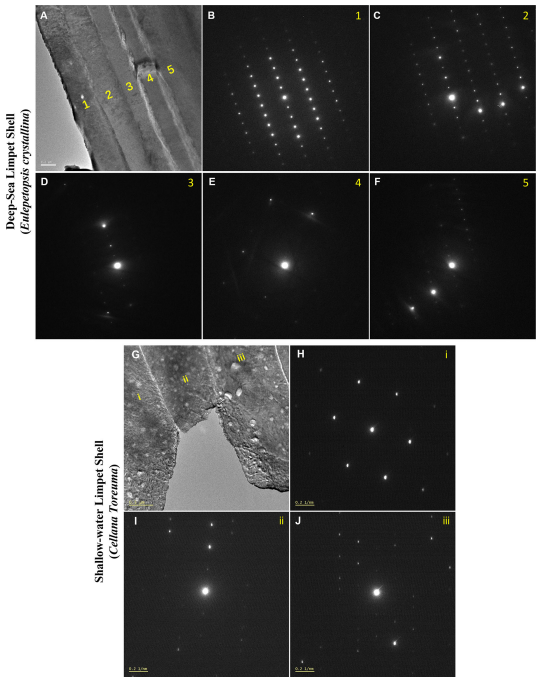

FIGURE 5
(A) The TEM image of the cross-sectional layered microstructures of deep-sea limpet *E. crystallina* shell. **(B–F)** Selected-area electron diffraction (SAED) patterns of the corresponding numbered layers 1–5 of deep-sea limpet *E. crystallina* shell in panel **(A)**. **(G)** The TEM image of the cross-sectional layered microstructures of shallow-water limpet *C. toreuma* shell. **(H–J)** SAED patterns of the corresponding numbered layers i–iii of shallow-water limpet *C. toreuma* shells in panel **(G)**.

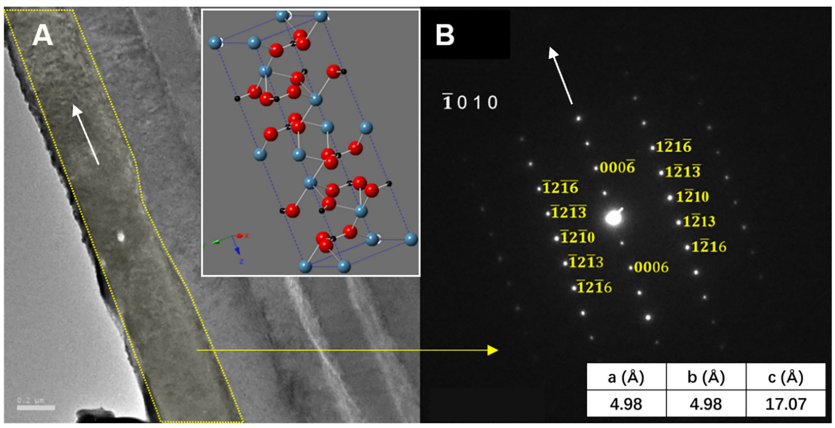

FIGURE 4
(A) The TEM image showing the crystallography of the inorganic phase of the deep-sea limpet *E. crystallina* shell and **(B)** SAED pattern of the marked area of the inorganic phase of the deep-sea limpet *E. crystallina* shell.

shells. In Figures 5H–J, SAED patterns verified that the crystal orientations of adjacent layered structures 1–3 were not aligned in a small tilt angle. For example, the diffraction patterns of layer 1 and neighboring layer 2 have no observable orientation relationship because *C. toreuma* limpet shells consist of two calcium carbonate crystal polymorphs and SAED patterns are no longer single crystal diffraction patterns, which will be discussed later together with the results of chemical composition.

EDS

The chemical composition refers to the chemical elements that make up the target material, which would clarify the marine living environment, cross-sectional layered structures, and crystalline arrangements. In general, the main chemical composition of marine animal shells is composed of carbonate minerals and some inorganic trace elements (Islam et al., 2011; Hamester et al., 2012; Wu et al., 2017). Regarding EDS characterization, the characteristic energy distribution spectra of X-rays can be obtained when samples are irradiated by electron beam, and thus EDS can determine most of elements in the sample qualitatively (Ying et al., 2021a). The elemental analysis of *E. crystallina* and *C. toreuma* shells was detected by energy-dispersive X-ray spectroscopy, and the EDS spectra (Figure 6) confirmed the presence of carbon (C), oxygen (O), magnesium (Mg), and calcium (Ca) in both *E. crystallina* and *C. toreuma* shells. Compared with *C. toreuma* shells (Figure 6B), *E. crystallina* shells uniquely obtained the trace of phosphorous (P) which originated from the potential phosphorite and phosphatic sediments in phosphorus-rich deep-sea vent ecosystems of the Southwest Indian Ocean (Figure 6A) (Baturin, 1982; Martin et al., 2018). Besides, the copper (Cu) signal originated from the TEM copper grid that was used for EDS measurements.

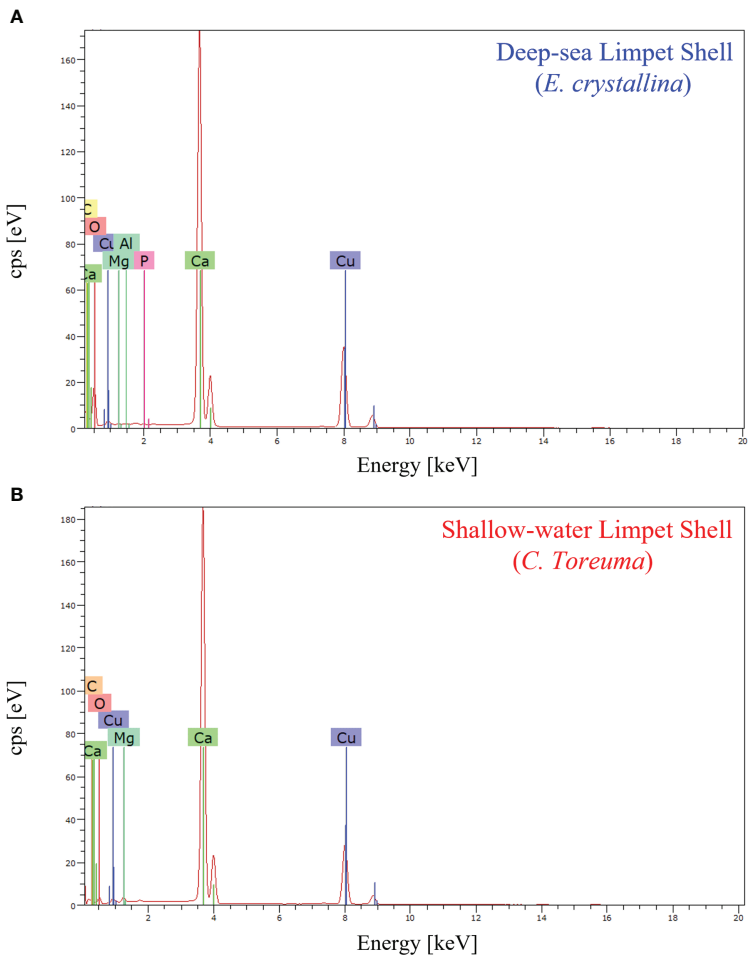

FIGURE 6
The EDS spectra of **(A)** deep-sea limpet *E. crystallina* shells containing Ca, C, and O as the main components and P and Al as unique trace elements and **(B)** shallow-water limpet *C. toreuma* shells containing Ca C, and O as the main components, where the Cu signal generates from the TEM copper grid used for EDS measurements.

FT-IR

The FT-IR spectra verified that *E. crystallina* shell and *C. toreuma* shell powder were composed of both organic substances and mineral compounds with characteristic bands from 4,000 cm^{-1} to 500 cm^{-1} (Kamalanathan et al., 2014). The prominent absorption peaks attributed to the CO_3^{2-} of calcite-$CaCO_3$ were observed at 1,045 cm^{-1}, 873 cm^{-1}, and 712 cm^{-1} in both *E. crystallina* and *C. toreuma* shells (Figure 7) (Cahya and Marfuah, 2014). Besides, the organic functional groups represented by the weaker absorption peaks were amide (2,520 cm^{-1}) and carboxylic acid (1,794 cm^{-1}) (Islam et al., 2011). *E. crystallina* shells contained unique phosphate (PO_4^{3-}) which was assigned to the broad IR absorption band at 1,100–1,200 cm^{-1} (Figure 7A) (Berzina-Cimdina and Borodajenko, 2012). In addition, the characteristic IR absorption peak of aragonite-$CaCO_3$ was observed at 1,082 cm^{-1} of CO_3^{2-} in *C. toreuma* shells (Figure 7B), which meant that the shallow-water limpet shell contained two type polymorphs of calcium carbonate (Lee et al., 2011). Besides, the amorphous calcium carbonate (ACC) was not found in TEM studies of both *E. crystallina* and *C. toreuma*, and this result can be further verified by the obtained FT-IR and XRD results of limpet powders (Figures 7, 8). In FT-IR spectra, the ACC is expected to show an evident shoulder peak on the main asymmetric ν_3 CO_3 band at 1,460 cm^{-1} (Wang et al., 2009), while this characteristic peak was not found in FT-IR spectra of *E. crystallina* and *C. toreuma* shells (Figure 7). In XRD spectra, the ACC is expected to feature two broad humps at approximately 30° and 45° 2θ (Rodriguez-Blanco et al., 2012), while these broad characteristic peaks were not shown in the XRD spectra of *E. crystallina* and *C. toreuma* shells (Figure 8).

XRD

The further powder XRD analysis (Figure 8) was conducted to determine all possible crystalline phases of $CaCO_3$ in the whole deep-sea and shallow-water limpet shells. XRD is generally used for phase identification of a crystalline material and can provide information on unit cell dimensions, characterization of

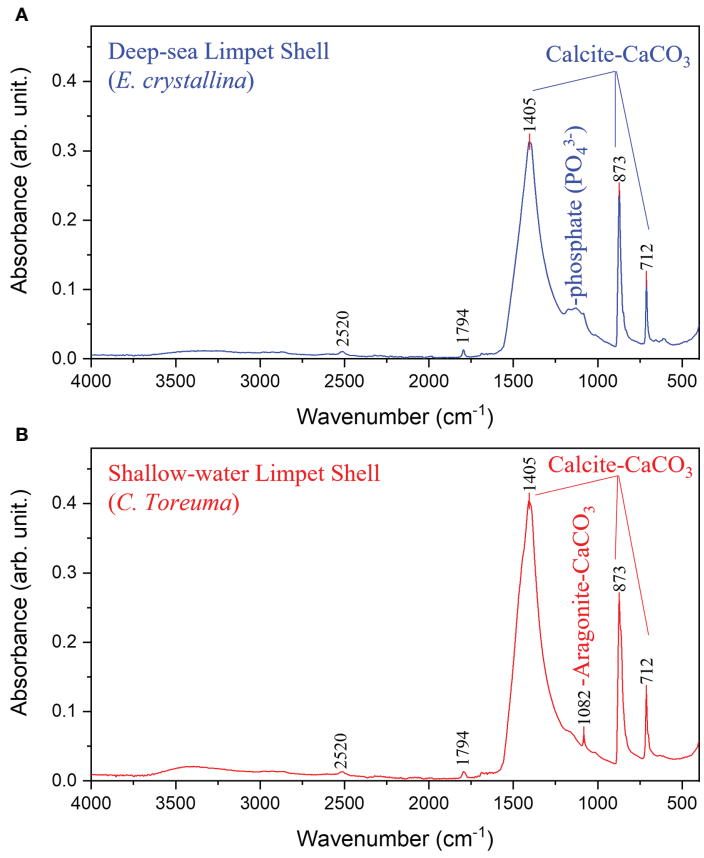

FIGURE 7
The FT-IR spectra of **(A)** deep-sea limpet *E. crystallina* shells containing calcite-$CaCO_3$ and unique phosphate (PO_4^{3}) and **(B)** shallow-water limpet *C. toreuma* shells containing two $CaCO_3$ polymorphs, calcite-$CaCO_3$ and aragonite-$CaCO_3$.

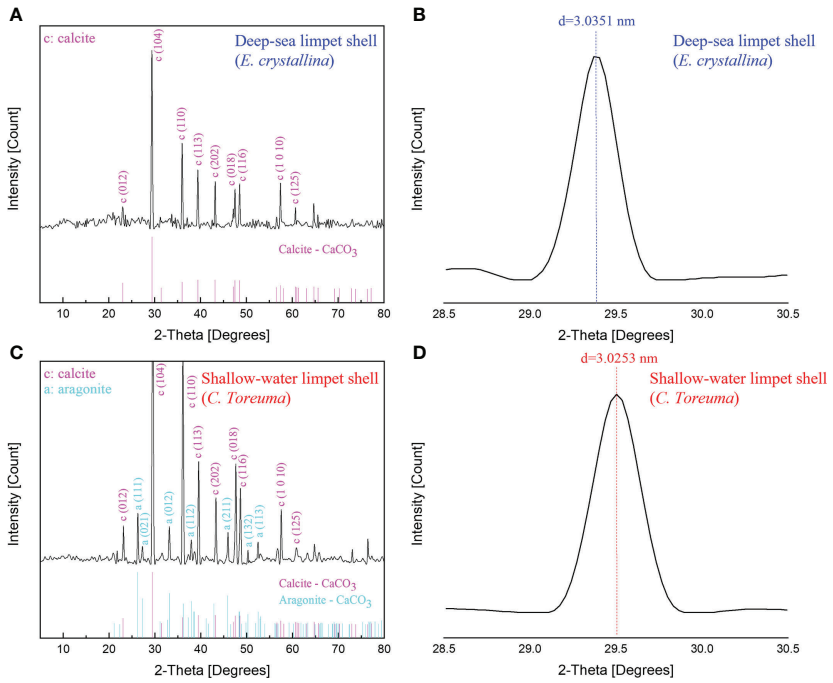

FIGURE 8
The XRD spectra of **(A)** deep-sea limpet *E. crystallina* shells containing pure calcite-$CaCO_3$. **(B)** The detailed diffraction peak information of deep-sea limpet *E. crystallina* shells which is consistent with the literature value. **(C)** Shallow-water limpet *C. toreuma* shells containing two types of $CaCO_3$ polymorphs, i.e., calcite and aragonite. **(D)** The detailed diffraction peak information of shallow-water limpet *C. toreuma* shells deviated from the literature value.

crystalline, and measurement of sample purity. According to the XRD results shown in Figure 8A, the phase of the powders obtained from *E. crystallina* shells was indexed to be a rhombohedral calcite–$CaCO_3$ structure which was consistent with the previous study (Duquette et al., 2017). The calcite–$CaCO_3$ phase features a rhombohedral structure with the calculated parameters of a = 4.98 Å, c = 17.07 Å, catalogized in space group R-3c (JCPDS card no. 01-080-9776) (Wu et al., 2017). The diffraction peaks of calcite were intense, and thus the powders were proven to be highly crystalline. The characteristic calcite-$CaCO_3$ peak of *E. crystallina* shells at 2θ of 29.4 ± 0.01° (Figure 8B) corresponded to the (1 0 4) crystallographic plane with the interplanar spacing d(*E. crystallina*-calcite) = 3.0351 ± 0.0003 nm which was consistent with the literature value of calcite crystal, d(calcite) = 3.0350 nm (Yuan et al., 2016). Notably, no diffraction peaks of other $CaCO_3$ polymorphs are detected, which confirmed the only high pure phase of calcite-$CaCO_3$ as the main composition in *E. crystallina* shells. In XRD spectra of *C. toreuma* limpet shells (Figure 8C), two polymorphs of calcium carbonate, i.e., calcite, aragonite, are detected as the crystalline phases. There are some small peaks confirming the existence of orthorhombic aragonite as a minor phase in *C. toreuma* shells with the lattice parameters a = 4.97 Å, b = 7.96 Å, c = 5.75 Å, catalogized in space group Pmcn (JCPDS card no. 01-075-9984) (Wu et al., 2017). However, the (1 0 4) calcite-$CaCO_3$ peak of *C. toreuma* shells at 2θ of 29.5 ± 0.01° (Figure 8D) corresponded to the interplanar spacing d(*C. toreuma*-calcite) = 3.0253 ± 0.0003 nm which is lower than the literature value of calcite (Yuan et al., 2016). The deviation of diffraction peaks resulted from the mixture of different $CaCO_3$ crystal polymorphs. The results from EDS, FT-IR, and XRD will provide more detailed chemical composition information on the demineralized isolation of molluscan conchixes and their potential multifunctional applications in pharmacy, cosmetics, and feed additives (Ehrlich et al., 2020).

Discussion

By using the TEM, SEM, FIB, EDS, and XRD techniques, the microstructure, crystallography, and chemical composition of deep-sea limpet *E. crystallina* shells living at a depth of 2,700 m of the Southwest Indian Ocean Ridge and shallow-water limpet *C. toreuma* shell were investigated and compared, which revealed effects of the living environment of ultra-high hydrostatic pressure on shell microstructures of deep-sea animals. Besides, the distinctive layered structures and pure calcite component of deep-sea limpet *E. crystallina* shells provided potential explanation of the origin of invertebrate marine biomaterials and further offered

prospective applications in forced biomineralization and extreme biomimetics.

Conclusions

In the present study, we conducted TEM, SEM, EDS, XRD, and FT-IR for the first time to investigate the shell microstructural features and chemical composition of the deep-sea limpet E. crystallina collected at a depth of around 2,700 m in the Southwest Indian Ocean Ridge. The results revealed the detailed layered microstructures, the exfoliation characteristics, and the tilted crystallographic orientation of each layer's unit cell at a small angle sequentially. The microscopic results further revealed that the E. crystallina shell exhibited untruncated and width-compressed layered structures due to the ultra-high hydrostatic force in the 2,700 m deep-sea condition, which disclosed potential effects of the living environment on the microstructure of deep-sea marine animal shells. Compared with shells of shallow-water limpet *C. toreuma*, *E. crystallina* shells were unique in containing pure calcite as the only calcium carbonate composition and the trace of phosphate originated from the phosphorus-rich deep-sea vent of the Southwest Indian Ocean, which verified that the deep-sea living environment potentially affected not only microstructures but also the chemical composition of marine animal shells.

Data availability statement

The raw data supporting the conclusions of this article will be made available by the authors, without undue reservation.

Ethics statement

The animal study was reviewed and approved by The Ethics Committee of the Hong Kong University of Science and Technology.

Author contributions

NW and PQ conceived and designed the project. ZY, SW, XC, and SX performed microstructure experiments of shells. ZY and XF performed the chemical composition experiments of shells. WW collected samples. ZY and WW drafted the manuscript. ZY, SW, SX, and YC participated in data analysis. All authors contributed to the manuscript revision and approved it for submission and publication.

Funding

This work was supported by grants from the Southern Marine Science and Engineering Guangdong Laboratory (Guangzhou) (SMSEGL20SC01).

Acknowledgments

The authors acknowledge the financial support from the Southern Marine Science and Engineering Guangdong Laboratory (Guangzhou) (SMSEGL20SC01) and the technical support at the Materials Characterization and Preparation Facility of The Hong Kong University of Science and Technology.

Conflict of interest

The authors declare that the research was conducted in the absence of any commercial or financial relationships that could be construed as a potential conflict of interest.

Publisher's note

Supplementary material

The Supplementary Material for this article can be found online at: https://www.frontiersin.org/articles/10.3389/fmars.2022.902815/full#supplementary-material

References

Agbaje, O. B. A., Shir, I. B., Zax, D. B., Schmidt, A., and Jacob, D. E. (2018). Biomacromolecules within bivalve shells: Is chitin abundant? *Acta Biomater.* 80, 176–187. doi: 10.1016/j.actbio.2018.09.009

Aizenberg, J., Hanson, J., Koetzle, T., Weiner, S., and Addadi, L. (1997). Control of macromolecule distribution within synthetic and biogenic single calcite crystals. *J. Am. Chem. Soc.* 119 (5), 881–886. doi: 10.1021/ja9628821

Baturin, G. N. (1982). *Phosphorites on the sea floor* (Amsterdam, Netherlands: Elsevier).

Berzina-Cimdina, L., and Borodajenko, N. (2012). *Research of calcium phosphates using Fourier transform infrared spectroscopy*. (London: IntechOpen).

Cahya, M., and Marfuah, N. (2014). "Identification of Calcium carbonate (CaCO3) characteristics from different kinds of poultry eggshells using X-ray diffraction (XRD) and Fourier transformation infra-red (FTIR)" in *2014 international conference on physics and its applications (ICOPIA-14)* (Dordrecht, Netherlands: Atlantis Press).

Carroll, M., and Romanek, C. S. (2008). Shell layer variation in trace element concentration for the freshwater bivalve *Elliptio complanata*. *Geo Mar. Lett.* 28 (5-6), 369–381. doi: 10.1007/s00367-008-0117-3

Checa, A. G., Okamoto, T., and Ramírez, J. (2006). Organization pattern of nacre in pteriidae (Bivalvia: Mollusca) explained by crystal competition. *Proc. R. Soc B* 273 (1592), 1329–1337. doi: 10.1098/rspb.2005.3460

Denny, M. W. (2000). Limits to optimization: fluid dynamics, adhesive strength and the evolution of shape in limpet shells. *J. Exp. Biol.* 203 (17), 2603–2622. doi: 10.1242/jeb.203.17.2603

Duquette, A., McClintock, J. B., Amsler, C. D., Pérez-Huerta, A., Milazzo, M., and Hall-Spencer, J. M. (2017). Effects of ocean acidification on the shells of four Mediterranean gastropod species near a CO_2 seep. *Mar. pollut. Bull.* 124 (2), 917–928. doi: 10.1016/j.marpolbul.2017.08.007

Ehrlich, H. (2019). *Marine biological materials of invertebrate origin* (Cham, Switzerland: Springer).

Ehrlich, H., Bailey, E., Wysokowski, M., and Jesionowski, T. (2021). Forced biomineralization: A review. *Biomimetics* 6 (3), 46. doi: 10.3390/biomimetics6030046

Ehrlich, H., Martinović, R., Joksimović, D., Petrenko, I., Schiaparelli, S., Wysokowski, M., et al. (2020). Conchixes: Organic scaffolds which resemble the size and shapes of mollusks shells, their isolation and potential multifunctional applications. *Appl. Phys. A* 126 (7), 1–13. doi: 10.1007/s00339-020-03728-7

Ehrlich, H., and Nikolaev, A. (2017). "\Psychrophiles as sources for bioinspiration in biomineralization and biological materials science" in *Extreme Biomimetics* (Cham, Switzerland: Springer), 1–51.

Hamester, M. R. R., Balzer, P. S., and Becker, D. (2012). Characterization of calcium carbonate obtained from oyster and mussel shells and incorporation in polypropylene. *Mater. Res.* 15, 204–208. doi: 10.1590/S1516-14392012005000014

Harford, N., O'Connor, N., and Taylor, D. (2020). Impact resistance of limpet shells: a study of local adaptations. *Appl. Phys. A: Mater. Sci. Process.* 126 (9), 1–9. doi: 10.1007/s00339-020-03941-4

Harley, C. D., Denny, M. W., Mach, K. J., and Miller, L. P. (2009). Thermal stress and morphological adaptations in limpets. *Funct. Ecol.* 23 (2), 292–301. doi: 10.1111/j.1365-2435.2008.01496.x

Islam, K. N., Bakar, M. Z. B. A., Noordin, M. M., Hussein, M. Z. B., Abd Rahman, N. S. B., and Ali, M. E. (2011). Characterisation of calcium carbonate and its polymorphs from cockle shells (*Anadara granosa*). *Powder Technol.* 213 (1-3), 188–191. doi: 10.1016/j.powtec.2011.07.031

Jiang, T., Liu, H., Huang, D., Zhang, S., Li, Y., Gong, X., et al. (2014). Valley and band structure engineering of folded MoS_2 bilayers. *Nat. Nanotechnol.* 9 (10), 825–829. doi: 10.1038/nnano.2014.176

Johnson, A. B., Fogel, N. S., and Lambert, J. D. (2019). Growth and morphogenesis of the gastropod shell. *Proc. Natl. Acad. Sci.* 116 (14), 6878–6883. doi: 10.1073/pnas.1816089116

Kamalanathan, P., Ramesh, S., Bang, L., Niakan, A., Tan, C., Purbolaksono, J., et al. (2014). Synthesis and sintering of hydroxyapatite derived from eggshells as a calcium precursor. *Ceram. Int.* 40 (10), 16349–16359. doi: 10.1016/j.ceramint.2014.07.074

Lee, S. W., Jang, Y. N., and Kim, J. C. (2011). Characteristics of the aragonitic layer in adult oyster shells, *Crassostrea gigas*: structural study of myostracum including the adductor muscle scar. *Evid. Based Complement. Altern. Med.* 2011, 10. doi: 10.1155/2011/742963

Li, L., Kolle, S., Weaver, J. C., Ortiz, C., Aizenberg, J., and Kolle, M. (2015). A highly conspicuous mineralized composite photonic architecture in the translucent shell of the blue-rayed limpet. *Nat. Commun.* 6 (1), 1–11. doi: 10.1038/ncomms7322

Lomovasky, B. J., de Aranzamendi, M. C., and Abele, D. (2020). Shorter but thicker: analysis of internal growth bands in shells of intertidal vs. subtidal Antarctic limpets, nacella concinna, reflects their environmental adaptation. *Polar Biol.* 43 (2), 131–141. doi: 10.1007/s00300-019-02615-z

Marie, B., Joubert, C., Tayalé, A., Zanella-Cléon, I., Belliard, C., Piquemal, D., et al. (2012). Different secretory repertoires control the biomineralization processes of prism and nacre deposition of the pearl oyster shell. *Proc. Natl. Acad. Sci.* 109 (51), 20986–20991. doi: 10.1073/pnas.1210552109

Martin, P., Lauro, F. M., Sarkar, A., Goodkin, N., Prakash, S., and Vinayachandran, P. (2018). Particulate polyphosphate and alkaline phosphatase activity across a latitudinal transect in the tropical Indian ocean. *Limnol. Oceanogr.* 63 (3), 1395–1406. doi: 10.1002/lno.10780

Nakai, S., Miura, O., Maki, M., and Chiba, S. (2006). Morphological and habitat divergence in the intertidal limpet *Patelloida pygmaea*. *Mar. Biol.* 149 (3), 515–523. doi: 10.1007/s00227-005-0241-9

Oliveira, C. R. M., De Castro, L. M., Da Cruz Nazareth, M. A., Harayashiki, C. A. Y., and Castro, Í. B. (2020). Shell structure and composition alterations in the limpet *Lottia subrugosa* along a contamination gradient in the santos estuary, Brazil. *Ecol. Indic.* 115, 106417. doi: 10.1016/j.ecolind.2020.106417

Rodolfo-Metalpa, R., Houlbrèque, F., Tambutté, É., Boisson, F., Baggini, C., Patti, F. P., et al. (2011). Coral and mollusc resistance to ocean acidification adversely affected by warming. *Nat. Clim. Change* 1 (6), 308–312. doi: 10.1038/nclimate1200

Rodriguez-Blanco, J., Shaw, S., Bots, P., Roncal-Herrero, T., and Benning, L. G. (2012). The role of pH and mg on the stability and crystallization of amorphous calcium carbonate. *J. Alloys Compd.* 536, S477–S479. doi: 10.1016/j.jallcom.2011.11.057

Song, X., Liu, Z., Wang, L., and Song, L. (2019). Recent advances of shell matrix proteins and cellular orchestration in marine molluscan shell biomineralization. *Front. Mar. Sci.* 6, 41. doi: 10.3389/fmars.2019.00041

Sun, J., Zhou, Y., Chen, C., Kwan, Y. H., Sun, Y., Wang, X., et al. (2020). Nearest vent, dearest friend: biodiversity of tiancheng vent field reveals cross-ridge similarities in the Indian ocean. *R. Soc Open Sci.* 7 (3), 200110. doi: 10.1098/rsos.200110

Suzuki, M., Kameda, J., Sasaki, T., Saruwatari, K., Nagasawa, H., and Kogure, T. (2010). Characterization of the multilayered shell of a limpet, *Lottia kogamogai* (Mollusca: Patellogastropoda), using SEM–EBSD and FIB–TEM techniques. *J. Struct. Biol.* 171 (2), 223–230. doi: 10.1016/j.jsb.2010.04.008

Suzuki, M., Kogure, T., and Nagasawa, H. (2017). Studies on the chemical structures of organic matrices and their functions in the biomineralization processes of molluscan shells. *AGri Biosci. Monogr.* 7, 25–39. doi: 10.5047/agbm.2017.00702.0025

Suzuki, M., Kogure, T., Weiner, S., and Addadi, L. (2011). Formation of aragonite crystals in the crossed lamellar microstructure of limpet shells. *Cryst. Growth Des.* 11 (11), 4850–4859. doi: 10.1021/cg2010997

Wang, X., Kong, R., Pan, X., Xu, H., Xia, D., Shan, H., et al. (2009). Role of ovalbumin in the stabilization of metastable vaterite in calcium carbonate biomineralization. *J. Phys. Chem. B* 113 (26), 8975–8982. doi: 10.1021/jp810281f

Wang, Y., Liu, C., Du, J., Huang, J., Zhang, S., and Zhang, R. (2018). The microstructure, proteomics and crystallization of the limpet teeth. *Proteomics* 18 (19), 1800194. doi: 10.1002/pmic.201800194

Weiner, S., and Addadi, L. (2011). Crystallization pathways in biomineralization. *Annu. Rev. Mater. Res.* 41, 21–40. doi: 10.1146/annurev-matsci-062910-095803

Wu, S., Chiang, C., and Zhou, W. (2017). Formation mechanism of $CaCO_3$ spherulites in the myostracum layer of limpet shells. *Crystals* 7 (10), 319. doi: 10.3390/cryst7100319

Ying, Z., Diao, J., Wang, S., Cai, X., Cai, Y., Liu, H., et al. (2020). Revealing high temperature stability of platinum nanocatalysts deposited on graphene oxide by in-situ TEM. *Mater. Charact.* 170, 110706. doi: 10.1016/j.matchar.2020.110706

Ying, Z., Diao, J., Wang, S., Cai, X., Cai, Y., Liu, H., et al. (2021a). *In situ* atomic-scale studies of thermal stability and surface reconstruction of ZnO nanowires based pd nanocatalysts. *Mater. Des.* 209, 109947. doi: 10.1016/j.matdes.2021.109947

Ying, Z., Diao, J., Wang, S., Cai, X., Cai, Y., Liu, H., et al. (2021b). Thermal stability, ripening dynamics and coalescing microstructures of reduced graphene oxide-based platinum nanocatalysts: An in-situ TEM study. *Diam. Relat. Mater.* 120, 108690. doi: 10.1016/j.diamond.2021.108690

Ying, Z., Diao, J., Wang, S., Cai, X., Liu, H., and Wang, N. (2021c). In-situ transmission electron microscopy: electron beam effects in carbon-based nanomaterials. *Microsc. Microanal.* 27 (S1), 2110–2113. doi: 10.1017/S1431927621007625

Yuan, K., Lee, S. S., De Andrade, V., Sturchio, N. C., and Fenter, P. (2016). Replacement of calcite ($CaCO_3$) by cerussite ($PbCO_3$). *Environ. Sci. Technol.* 50 (23), 12984–12991. doi: 10.1021/acs.est.6b03911